ELSEVIER

Materials Science and Engineering A 435–436 (2006) 212–220

MATERIALS SCIENCE & ENGINEERING A

www.elsevier.com/locate/msea

Effect of initial powder morphology on thermal and mechanical properties of stand-alone plasma-sprayed 7 wt.% Y_2O_3–ZrO_2 coatings☆

Batur Ercan[b], Keith J. Bowman[a], Rodney W. Trice[a,*], Hsin Wang[c], Wally Porter[c]

[a] *School of Materials Engineering, Purdue University, West Lafayette, Indiana 47907-2044, United States*
[b] *Division of Engineering, Brown University, Providence, RI 02912, United States*
[c] *Oak Ridge National Laboratory, Oak Ridge, Tennessee 37831-6087, United States*

Received 1 May 2006; received in revised form 21 June 2006; accepted 21 July 2006

Abstract

The effects of starting powder morphology on the thermal and mechanical properties of stand-alone plasma-sprayed 7 wt.% Y_2O_3–ZrO_2 (YSZ) coatings were studied. Two powder morphologies were investigated: an agglomerated and sintered powder (referred to presently as "AS") and a powder manufactured using plasma spheroidization to create hollow spheres (referred to presently as "HS"). Coatings made from AS powders contained 0.21 wt.% SiO_2 impurity, twice as much as observed in coatings made from HS powders. Properties of coatings made from each powder type were compared in the as-sprayed state and after 50 h heat treatments at temperatures ranging from 1000 to 1400 °C.

SEM microstructural investigations revealed significant differences in the porosity and distribution of pores in the coatings. In coatings made with AS powders the majority of the high aspect ratio pores were located between lamella (interlamellar porosity). In addition to interlamellar pores, coatings made with HS powders demonstrated 1.5 times more spherical-shaped globular pores by number located within lamella. Globular pores were shown to still exist in coatings made with HS powders after 50 h heat treatments at 1400 °C. Archimedes porosity measurements showed that coatings made with AS powders typically contained 4–5% less total porosity than coatings made with HS powders.

Thermal conductivity experiments using laser flash showed that there was no difference in the thermal conductivity of coatings made from either powder type in the as-sprayed state despite higher porosity in the coatings made from HS powders. After a 50 h heat treatment at 1000 and 1200 °C, coatings made from both powder types still demonstrated statistically similar thermal conductivities. However, after a 50 h heat treatment at 1400 °C the thermal conductivity of coatings made from AS powders was found to be 0.3 W/m/K higher than coatings made from HS powders. Microstructural differences in the coatings made from the two powder types that affected sintering rates, including the increased level of SiO_2 impurities and fewer globular pores, were used to explain variations in properties.

In uniaxial compression tests on stand-alone samples at 1000, 1100, and 1200 °C, coatings made from AS powders typically relaxed more stress than coatings made from HS powders. Differences in coating relaxation became more apparent as the test temperature increased through 1200 °C. The higher percentage of impurity SiO_2 in the AS coatings is believed to contribute to increased relaxation via formation of a glassy phase at the grain boundaries which assists grain boundary sliding during elevated temperature deformation.

Keywords: Thermal barrier coatings; Zirconia; Thermal properties; Mechanical properties; Yttria-stabilized zirconia

1. Introduction

Thermal barrier coatings (TBCs) are thin ceramic coatings applied to the surface of metallic structures in gas turbine engines exposed to high-temperatures [1–4]. A TBC system consists of two different layers. The bottom layer is a ~100 μm thick MCrAlY (M stands for Ni, or Co) or PtAl intermetallic bondcoat applied on a superalloy [5]. The topcoat is often a ~200 μm thick layer of 7 wt.% Y_2O_3–ZrO_2 (YSZ). One common method for applying the YSZ topcoat is plasma spray. In this method, YSZ powders are carried by an inert gas mixture into a plasma plume where they are melted, accelerated, and propelled against a substrate. The molten particles impact and solidify on the substrate creating the characteristic layered lamellar microstructure with a typical porosity of 10–20% [3]. The microstructure of a plasma-sprayed coating contains three main defect types: intralamellar

☆ This work was supported by the National Science Foundation through DMR-0134286.
* Corresponding author. Tel.: +1 765 494 6405.
E-mail address: rtrice@purdue.edu (R.W. Trice).

0921-5093/$ – see front matter © 2006 Elsevier B.V. All rights reserved.
doi:10.1016/j.msea.2006.07.085

cracks, interlamellar pores and globular pores [6]. Intralamellar cracks, which are oriented parallel with the spray direction and typically cut through individual lamellae, are formed during cooling by thermally induced stresses that form in the plane of the coating. High aspect ratio interlamellar pores are formed at the lamella boundaries, and are oriented primarily perpendicular to the spray direction. Spherical-shaped globular pores are located within individual lamella. Both interlamellar and globular pores result from gas entrapment during plasma-spraying [1]. In the former case, the gas is trapped between lamella, and in the latter case, the gas is trapped in the melted particle. Porosity can also result from inefficient packing of the melted droplets as they stack on top of one another.

One of the most important parameter affecting the properties of TBCs is starting feedstock powder morphology. Three powder morphologies are primarily used to produce coatings: agglomerated and sintered, fused and crushed, and plasma-spheroidized. In the first type, powders are often spray-dried to agglomerate many submicron powders into larger size powders (typically $\geq$20 μm), followed by a sintering step that removes a portion, but not all, of the porosity between the smaller powders [7]. Powders produced using this method are referred to presently as AS and contain small micro-pores between the submicron powders comprising the large powder. Solidified dense ingots that are consequently crushed into a powder (i.e. fused and crushed) are referred to presently as FC. Powders of this type typically have no internal porosity. Plasma-spheroidized powders, are made by plasma-spraying agglomerated and sintered powders such that typically only the outer surface melts, trapping single large pores in the middle of each powder [8]. The morphology in these powders, which are referred to as HS, is one of a hollow sphere.

Different initial powder morphologies have been shown to result in different coating structures and properties after plasma-spraying. In a study by Ilavsky and Stalick [9] using neutron diffraction, they showed that powders with identical starting composition (i.e. 7 wt.% Y_2O_3–ZrO_2) but in different powder morphologies exhibited different phase constituents after plasma spray. Coatings made from HS powders were 24 wt.% c-ZrO_2, while coatings produced from FC powders contained 6 wt.% c-ZrO_2. The starting powder morphology can also affect the mechanical properties of a plasma-sprayed coating. For example, Wallace and Ilavsky [10] showed that the elastic modulus of coatings sprayed from HS powders was higher than coatings sprayed from FC powders, despite having higher porosity. Orientation specific behavior and planar defect surfaces (i.e. interlamellar porosity) perpendicular to the indentation direction were found to be the largest contributing factors to decreasing elastic modulus values in coatings made from FC powders. Allen et al. [11] showed that in coatings made from FC and HS powders that were then subject to 1 h heat treatment at 1400 °C had considerably different cross-sectional microstructures. It was found that coatings made from FC powders partially retained their lamellar structure while the coatings made from HS powders lost nearly all its lamellar structure. Thus, the starting powder morphology can affect sintering rates and sintered microstructures.

The primary function of a TBC is to protect the underlying metallic structure from temperature extremes by imposing a temperature gradient through its thickness. The key property that determines its ability to perform this task is its thermal conductivity. In order to decrease the thermal conductivity, a variety of different approaches have been investigated. Adjusting the spraying parameters, addition of a low thermal conductivity second phase [12], multi-component defect clustering approach [13], doping with trivalent and pentavalent oxides [14] are examples of some of the approaches tried to date. In research conducted by Kulkarni et al. [15], the thermal conductivities of coatings sprayed from FC, AS, and HS powders were compared with each other. The thermal conductivities were found to be 0.95 ± 0.02, 0.89 ± 0.02, and 0.64 ± 0.01 W/m/K, respectively. It is worth noting that coatings made from AS powders had higher porosity than coatings made from HS powders, yet had a higher thermal conductivity. Broad particle size distribution and hollow sphere morphology of the HS powders were suggested as possible reasons for its lower thermal conductivity.

In the current research, the thermal conductivity and stress–relaxation behavior of 7 wt.% Y_2O_3–ZrO_2 coatings made from AS and HS powders are compared in the as-sprayed state and after 50 h heat treatments at 1000, 1200, and 1400 °C. Laser flash was used to determine the thermal conductivity while an uniaxial compression stress–relaxation test performed on stand-alone coatings was used to assess the high-temperature mechanical behavior of coatings made from different powder types. Heat treatments at different temperatures prior to thermal and mechanical testing were used to characterize the change of properties in each coating type due to sintering.

2. Experimental procedure

2.1. Powder description and characterization

Two starting powders with different morphologies were investigated. The first was an agglomerated and sintered (AS) powder.[1] The second powder type was a hollow sphere (HS) morphology produced via plasma spheroidization.[2] A spray-dried powder morphology served as the starting point in the production of both AS and HS powders. By manipulation of subsequent processing steps the distribution of porosity was intentionally varied. In the AS powders the collection of submicron powders were sintered so very small pores were spread through out the powder cluster; in the HS powders the starting collection of submicron powders were plasma-densified so one big central pore was formed within a powder. Cross-sectional views of AS and HS powders are shown in Fig. 1a and b. Powder size distributions were determined by a Microtrac brand laser light diffraction particle size distribution analyzer[3] at Praxair Surface Technologies Inc. Both of the powder types had the same d_{50} (~58 μm), but AS powders had a wider particle size distribution than HS powders.

[1] Praxair Surface Technologies, Indianapolis, IN, part number AS-1075.
[2] Praxair Surface Technologies, Indianapolis, IN, part number ZrO_2-317HS.
[3] Microtrac, North Largo, Florida.

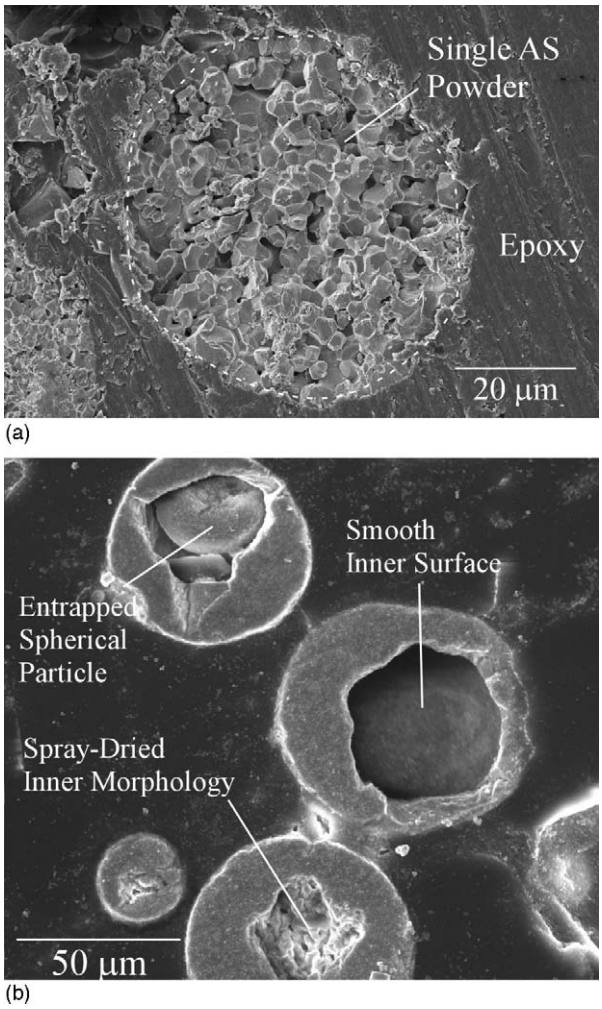

Fig. 1. SEM images of polished cross-sectional views of: (a) AS powder mounted in epoxy and (b) HS powder mounted in epoxy.

2.2. Sample fabrication

Cylindrical and flat samples were prepared with AS and HS powders using an SG-100 torch connected to an ABB IRB-2400 seven axis robot.[4] Cylindrical samples were used for stress–relaxation experiments while flat samples were employed for laser flash studies. The spraying parameters for AS and HS powders are shown in Table 1. The difference in spray parameters is due to the morphology of the starting powders. Coatings made from both powders were sprayed with a stand-off distance of 203.2 mm. Coatings made from AS powders used a gun power of 22.5 kW and powder feed rate of 53 g/min, whereas coatings made from HS powders used a gun power of 35 kW and 60 g/min powder feed rate.

Cylindrical specimens were made by plasma-spraying on rotating tubular-shaped aluminum substrates. The plasma gun was traversed up and down the 254 mm long and 12.7 mm outer diameter tube at a rate of 1181 mm/s. The cylindrical substrate was cooled during plasma-spraying by a ∼0.689 MPa air-knife placed at a 50.8 mm standoff behind the substrate. Coatings made from AS and HS powders required 240 and 200 cycles, respectively, to achieve comparable coating thicknesses (∼500 μm).

Table 1
Spraying parameters for coatings made with AS and HS powders

Spray parameters	AS coatings	HS coatings
Feed	Internal	External
Primary current	450 A	700 A
Secondary current	225 A	250 A
Gun power	22.5 kW	35 kW
System voltage	54.8 V	55.6 V
Primary gas flow rate (Ar)	58 l/min	41.5 l/min
Carrier gas flow rate (Ar)	2.8 l/min	1.9 l/min
Feed rate	53 g/min	60 g/min
Stand-off	200 mm	200 mm

Flat coating specimens of both powders types were produced by plasma-spraying on aluminum substrates with dimensions of 76.2 mm × 76.2 mm × 6.35 mm. The robot arm traversed the substrate at 500 mm/s. Coatings made from AS powders took seven cycles to build-up the desired coating thickness, with each cycle traversing the substrate completely in both horizontal and vertical dimensions. Coatings made from HS powders took eight cycles for comparable coating build-up.

Specimen preparation steps for cylindrical coatings have been described in detail in prior research [16]. Briefly, coated 254 mm long rods were sectioned into multiple cylinders and a weak HCl solution was used to leach out the aluminum substrates, leaving cylindrical stand-alone plasma-sprayed cylindrical coatings 12.5–16 mm in height. Cylindrical samples were used for mechanical testing. Flat specimens were produced using a circular diamond core drill, followed by removal of the aluminum substrate using a weak HCl solution. Stand-alone plasma-sprayed flat specimens were ∼0.45 mm thick and either 5 or 13 mm diameter were prepared. The smaller diameter samples were used to determine the specific heat of the YSZ while the larger diameter samples were used for laser flash experiments. Coatings made from each powder type were pulverized and chemically analyzed using inductively coupled plasma.

2.3. Sample characterization

The bulk density of each coating type and geometry was measured using Archimedes' method [17]. Using a theoretical density of 6.08 g/cm^3 for dense YSZ [18], the total porosity was also calculated. Prior to thermal and mechanical evaluation, some of the stand-alone coatings were heat treated. Heat treatments of cylindrical coatings of both powder types were conducted at 1200 °C for 50 h while heat treatments of flat specimens were carried out at 1000, 1200 or 1400 °C for 50 h. Using micrometers, the percentage change in height of coatings was measured before and after heat treating.

Scanning electron microscope investigations of the two starting powders, and coatings in the as-sprayed and after heat treatment were conducted. A ∼6 nm thick gold–palladium film was sputtered on samples to avoid charging during investiga-

[4] Asea Brown Boveri, Madrid, Spain.

tion. A Hitachi S4800 field emission SEM and Electroscan ESEM-2020 were used to take the micrographs. The number of globular shaped pores was quantitatively determined for coatings made from each powder type from 15 randomly chosen cross-sectional areas. The area that was investigated in each image was ~0.45 mm^2.

2.4. Thermal conductivity measurements

A detailed description of the laser flash technique used to determine thermal diffusivity has been published previously [19]. Coatings made from each powder type were investigated. All measurements were made at the High Temperature Materials Laboratory at the Oak Ridge National Laboratory. Thermal diffusivity measurements between 100 and 1200 °C were conducted using an Anter type FL5000 multiple laser thermal diffusivity system using 13 mm diameter stand-alone flat coatings. This system is equipped with a movable Nd:glass laser unit with a pulse energy up to 35 J and laser wavelength of 1.06 μm and two IR detectors. Experiments conducted at temperature ranges of 100–500 °C were with an aluminum furnace while measurements from 650 to 1200 °C were made with a graphite furnace. The time–temperature curves for individual samples were analyzed by the method of Clark and Taylor [20]. Both sides of the laser flash specimens were coated with graphite to make them opaque to the laser used for heating. Three measurements of thermal diffusivity were taken for each sample at each temperature and averaged. At least three replicates for each testing condition were performed.

Specific heat was determined from 100 to 1050 °C for coatings made from each powder type using a differential scanning calorimeter using sapphire as the reference standard. The heat-up rate was 20 °C/min in an atmosphere of argon. Samples were 5 mm in diameter and stacked to achieve a mass of 0.90 mg.

Once the diffusivity and specific heat were determined, the thermal conductivity of each sample was calculated using the following equation:

$$k_{\text{th}}\,(\text{W/m/K}) = \alpha\,(\text{cm}^2/\text{s}) \times c_p(\text{J/g/K}) \times \rho\,(\text{g/cm}^3) \times 100 \quad (1)$$

where k_{th} is the stands for thermal conductivity, α the thermal diffusivity, c_p the heat capacity and ρ is the bulk density of the material with units noted. Density was assumed constant for the current measurements. The total error associated with each thermal conductivity value is ±5%.

2.5. Stress–relaxation testing

High-temperature compression testing was performed using a servo-hydraulic load frame[5] equipped with hydraulic collet grips, an alignment fixture,[6] a 100 kN force transducer, SiC pushrods, and a high-temperature furnace.[7] Strain was measured with a high-temperature extensometer[8] with a resolution of ±1 μm. The design of the extensometer was such that an alumina pushrod extended vertically through the center of the lower SiC pushrod, through a small hole in the lower SiC compression platen, through the hollow stand-alone YSZ sample, and to the surface of the upper SiC pushrod. Strain was measured as the extensometer recorded any displacement between the stationary upper compression platen and the cantilever supporting the pushrod. The distance between the upper platen and the cantilever under an applied load was governed by the material response of the stand-alone coating between the platens. Alignment of the load frame was adjusted prior to testing the coatings to ensure that load was distributed equally around the circumference of the sample. A full description of the alignment procedure is available in Ref. [16].

Stress–relaxation tests were performed on stand-alone coatings made from each powder type at temperatures ranging from 1000 to 1200 °C and an initial compressive stress of 40 MPa. Some samples were heat treated for 50 h at 1200 °C prior to testing. Each sample was heated to the desired temperature at a rate of 10 °C/min under no applied load. After the target temperature was reached and stabilized for 15 min, the test was initiated by monotonically increasing the stress applied to the YSZ tube at a rate of 20 N/s to a pre-determined initial stress. Once 40 MPa was reached, the control system was rapidly changed from force to strain feedback, and the strain was held constant for 3 h. The material response was measured by observing the stress reduction with time. The noise in the load signal represents ±1 MPa uncertainty. Thermal expansion of the YSZ tubes and the load frame did not influence the material response, as no load was applied during heating or during the 15 min stabilization period. Three replicates for each coating type and condition were tested and averaged.

2.6. Stress–relaxation modeling

Three individual Maxwell elements arranged in parallel, where a Maxwell element consists of an elastic spring and viscous dashpot in series, were used to model the stress–relaxation of plasma-sprayed YSZ coatings made from both powder types [16]. Prior work showed that three Maxwell elements are required to model coatings that do not completely stress–relax within the 3 h test [16]. Mathematically this is represented by:

$$\sigma(t) = \sigma_0 \sum_{k=1}^{n} w_k \exp\left(-\frac{t}{\tau_k}\right) \quad (2)$$

and

$$\sum_{k=1}^{n} w_k = 1 \quad (3)$$

where σ_0 is the initial stress, n the number of Maxwell elements in parallel, w_k a weighting factor that is summed to unity, and

[5] MTS 810 Load Frame, Minneapolis, MN.
[6] MTS 609 Alignment Fixture, Minneapolis, MN.
[7] Applied Test Systems Inc., High Temperature Furnace, Butler, PA.
[8] MTS 632.70H-01, Minneapolis, MN.

t is the time. The time constant for each Maxwell element, τ_k, can be further defined as:

$$\tau_k = \frac{\eta_k}{E_k} \tag{4}$$

where η_k is the viscosity of the dashpot and E_k is the modulus of the spring for each Maxwell element.

Individual τ_k and w_k were fit to a given set of experimental data using a least-squares curve fitting method by minimizing R as defined in the following equation:

$$R = \sum_{t=0}^{t=t_f} \sqrt{|[\sigma_{exp}(t)]^2 - [\sigma_{mod}(t)]^2|} \tag{5}$$

where $\sigma_{exp}(t)$ and $\sigma_{mod}(t)$ represent stress values obtained experimentally and from numerical modeling, respectively, from the start of the test ($t=0$) until the end of the test ($t=t_f$). The R value has no physical meaning, but is minimized to provide the best fit of the model to the experimental data. Stress values were squared to give higher stress values greater weight in determining a proper fit. The square root of this difference for each time-step is summed over the complete test time, yielding an R value. This value can be minimized by iteratively varying τ_k and w_k and thereby providing the best fit of the model to the experimental stress–relaxation data.

3. Results

3.1. Microstructural characterization of coatings in the as-sprayed condition

The average thickness, bulk density, and open, closed and total porosity of as-sprayed stand-alone flat and cylindrical coatings made from both powder types are presented in Table 2. For flat samples, entries in Table 2 represent approximately 30 samples. Similarly, for cylindrical samples each entry represents approximately 60 samples that were measured and averaged. Most of the porosity was of the open type, and flat coatings were typically less dense (i.e. more total porosity) than cylindrical sample of the same powder type.

The chemical compositions of coatings made from AS and HS powders as determined by inductively coupled plasma are given in Table 3. The impurity level in coatings made from AS powders was higher than the impurity level in coatings made with HS powders. In particular, the SiO_2 content of the coatings made from AS powders was 0.210 wt.% as compared to 0.095 wt.% for coatings made from HS powders. Silica is a well known glass former. Calcium, which can act to modify the silica network, also appeared in greater concentration in coatings made from the AS powder.

Table 2
Average physical properties of all as-sprayed coatings made with AS and HS powders

Coating geometry	Property	AS coatings	HS coatings
Flat	Plate thickness (mm)	0.45 ± 0.02	0.46 ± 0.01
	Bulk density (g/cm^3)	4.6 ± 0.2	4.3 ± 0.2
	Open porosity (%)	16.5 ± 2.1	21.7 ± 1.7
	Closed porosity (%)	7.4 ± 1.7	7.2 ± 2.6
	Total porosity (%)	23.9 ± 2.6	28.9 ± 2.5
Cylindrical	Tube thickness (mm)	0.45 ± 0.04	0.52 ± 0.08
	Bulk density (g/cm^3)	4.9 ± 0.1	4.7 ± 0.2
	Open porosity (%)	16.2 ± 2.3	20.7 ± 2.7
	Closed porosity (%)	3.7 ± 1.8	2.6 ± 1.3
	Total porosity (%)	19.6 ± 2.2	23.3 ± 2.5

The substrate geometry varied from a cylindrical to a flat geometry.

Table 3
Chemical compositions of plasma-sprayed coatings made from AS and HS powders obtained from ICP testing

Compounds and elements	AS coatings (wt.%)	HS coatings (wt.%)
Y_2O_3	6.70	7.28
HfO_2	1.62	1.88
Al_2O_3	0.24	0.11
SiO_2	0.210	0.095
Ca	0.01–0.1	0.001–0.01

Typical cross-sectional SEM micrographs of coatings made from AS and HS powders in the as-sprayed condition are shown in Figs. 2 and 3a revealed similarities and differences. Interlamellar porosity (between lamella) and intralamellar cracks were apparent in both; these features common to all plasma-sprayed coatings are not highlighted in this paper. The primary difference between coatings made with the two powder types is that more globular pores were apparent in coatings made with HS powders. Quantitative phase analysis conducted on multiple cross-sectional images of both coating types showed coatings made with AS powders to have an average of 4.8 globular pores per 0.45 mm^2 and coatings made with HS powders to have an average of 12.1 globular pores per 0.45 mm^2. Differences in globular pore concentration can be understood by considering the microstructures of the starting powders (see Fig. 1). While AS powders had numerous small pores spread homogeneously within the a single powder, HS powders tended to have a single big pore inside individual powders. Apparently, it is more difficult for the entrapped gas to escape in HS powders during spraying than in AS powders. Small angle neutron experiments

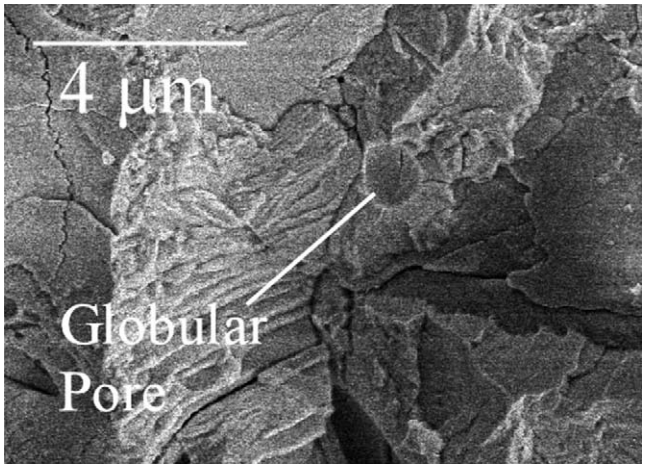

Fig. 2. SEM micrograph of the cross-section of an as-sprayed coating made from AS powders.

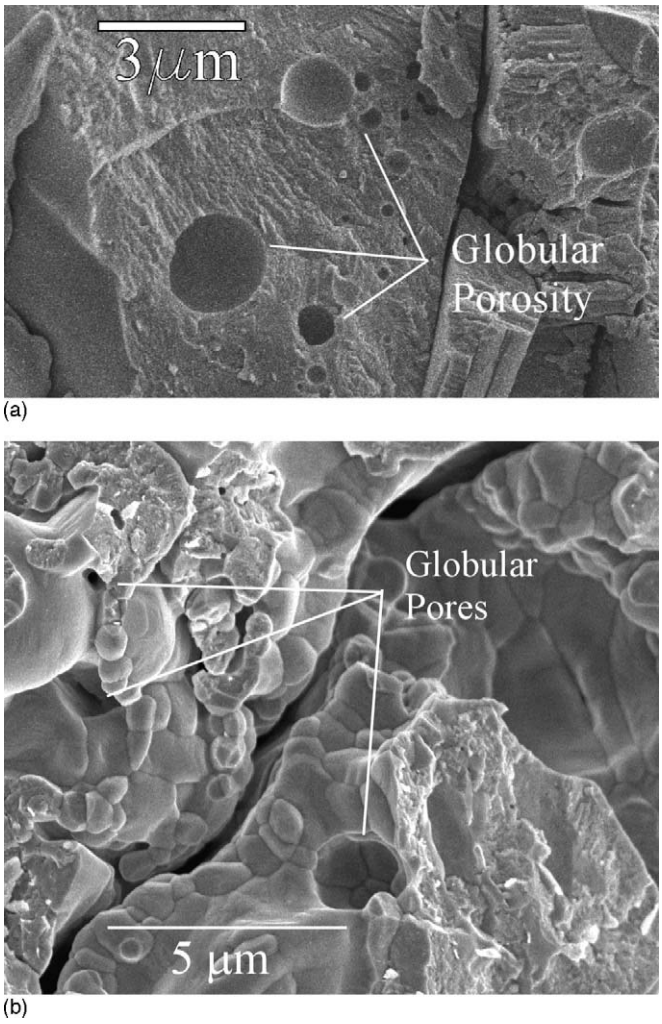

Fig. 3. SEM micrograph of the cross-section of a coating made from HS powders in the: (a) as-sprayed condition and (b) after a 50 h heat treatment at 1400 °C.

have observed similar large concentrations of globular shaped pores in coatings made with hollow-sphere powders [11].

3.2. Microstructural characterization of coatings after heat treatment

The percentage linear change in height of the cylindrical coatings was measured after a 50 h heat treatment at 1200 °C. It was calculated to be $0.29 \pm 0.05\%$ and $0.17 \pm 0.08\%$ for coatings made from AS and HS powders, respectively. This data shows that the general trend is that coatings made from AS powders sinter more than coatings made with HS powders. There are two plausible reasons for this behavior. Previous research has shown that SiO_2 content in YSZ has a major influence on sintering rate [21,22]. Studies conducted by Eaton et al. found a 5-fold increase in total shrinkage after a 24 h heat treatment at 1427 °C when the silica content of the YSZ was increased from 0.2% to 4%. As is well known, SiO_2 forms a silica-rich glassy phase at the grain boundaries and this can promote liquid-phase sintering [22]. As the SiO_2 impurity content in coatings made from AS powders was higher than that in coatings made from HS powders this could contribute to the observed behavior.

Secondly, the difference in porosity manifestation in the two coating types may play a role. Erk et al. [23] has shown using atomic force microscopy that interlamellar pores can completely close via grain boundary bridging across lamella. These pores are always connected to grain boundaries which serve as relatively fast diffusion paths during densification. Globular pores manifest themselves differently than interlamellar pores, typically residing within a grain (see Fig. 3a). Thus, the primary diffusion path is through the lattice, a much slower transport path. Thus, even though coatings made with HS powders contain more porosity, and thus would be expected to sinter more, the large component of globular pores in these coatings resisted sintering. Fig. 3b is a cross-sectional micrograph of a coating made from HS powders that has been heat-treated for 50 h at 1400 °C. It is evident that a large population of globular pores remain after the heat treatment. Prior SEM analysis on heat-treated coatings made via hollow sphere powders observed the same residual globular pores [24].

3.3. Thermal conductivity measurements

Fig. 4 presents a plot of the thermal conductivity of coatings measured from 100 to 1200 °C made from AS and HS powders after 50 h heat treatments at 1000, 1200, and 1400 °C. Not shown in Fig. 4 are the thermal conductivities of each coating type in the as-sprayed condition; for coatings made from either powder type the as-sprayed k_{th} values were statistically no different than the k_{th} measured after a 50 h heat treatment at 1000 °C.

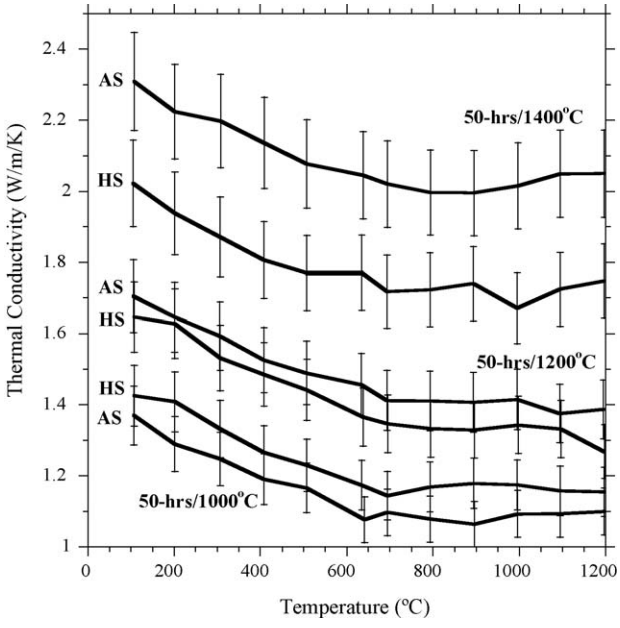

Fig. 4. Thermal conductivity of stand-alone as-sprayed and heat treated after 50 h heat treatments at 1000, 1200 and 1400 °C for coatings made from AS and HS powders. From graph bottom to top, the first and second lines represent the thermal conductivity after 50 h heat treatments at 1000 °C, the third and fourth lines represent the thermal conductivity after 50 h heat treatments at 1200 °C, and the fifth and sixth lines represent the thermal conductivity after 50 h heat treatments at 1400 °C.

It was observed that the k_{th} of coatings in the as-sprayed condition or after heat treatment at 1000 or 1200 °C for 50 h was not influenced by the starting powder type. This was true despite the fact that coatings made from HS powders were more porous than coatings made from AS powders, as shown in Table 2. In review, as-sprayed flat coatings made from AS and HS powders had total porosities of $23.9 \pm 2.6\%$ and $28.9 \pm 2.5\%$, respectively. Trice et al. [12] showed in plasma-sprayed YSZ that a 6% increase in porosity (i.e. from 12% to 18% total porosity) would correspond to a 0.4 W/m/K decrease in k_{th}. Thus, despite being more porous, coatings made from HS powders have statistically similar k_{th} to the more dense coatings made with AS powders.

An explanation for this behavior can be traced back to the manifestation of the globular pores in coatings made with HS powders. A heat-flux model developed by Kulkarni et al. [15] shows that defects perpendicular to the orientation of heat flow direction are the most effective to reduce thermal conductivity. In their study, they compared the heat flux through identical pore volumes, varying the aspect ratio of the pore from low (i.e. representative of a globular pore) to high (representative of an interlamellar pore). What they observed was that high aspect ratio pores, when oriented such that the long dimension was perpendicular to the predominant heat flow direction, were very effective in reducing k_{th}. This is because the effective cross-sectional area is much greater in the high aspect ratio pore than the low aspect ratio pore. Thus, despite the fact that coatings made from HS powders were less dense, the primary porosity type contributing to the difference in porosity between the two coating types was of the low-aspect ratio type. While low-aspect ratio pores reduce the thermal conductivity of a material, they do not do so as effectively as high aspect ratio pores oriented perpendicular to the heat flow.

As shown in Fig. 4, coatings made from the AS powder that were heat-treated for 50 h at 1400 °C demonstrate a statistically significant higher k_{th} as compared to coatings prepared with HS powders after identical heat treatments. XRD analysis of coatings prepared with AS and HS powders after the heat treatment did not indicate that any m-ZrO_2 phase had formed. Thus, the formation of a high thermal conductivity m-ZrO_2 phase was not responsible for the observed increase in thermal conductivity in coatings made from AS powders. One reason for increased k_{th} in coatings made with AS powders is extensive sintering of the high aspect ratio interlamellar pores. As discussed previously, the lenticular-shaped interlamellar pores, which are the main type of porosity in the AS coatings, sintered more completely than the globular pores that dominate in coatings made of HS powders. This behavior is in agreement with SANS data observed by Allen et al. [24] on coatings made with hollow sphere powders. However, the increased amount of silica content may also contribute to increased sintering in coatings prepared with AS powders, as observed by Eaton and Novak [21].

3.4. Stress–relaxation behavior

Stress–relaxation tests were conducted on cylindrical stand-alone coatings made from AS and HS powders in the as-sprayed state and after a 50 h heat treatment at 1200 °C. Coatings in both states were relaxed at 1000, 1100 or 1200 °C under an initial stress of 40 MPa. The results are presented in Fig. 5a and b. Tables 4 and 5 provide the magnitude of stress–relaxed in each regime along with the time constants associated with relaxation in both regimes for coatings made from the two different powders. As noted by Dickinson et al. [16], stress–relaxation behavior in plasma-sprayed YSZ follows two regimes: an ~10 min initial fast stress–relaxation regime, followed by a slower secondary relaxation regime for the remaining minutes of the test. The stress–relaxation data for coatings made from the two different powders in the as-sprayed and heat treated condition showed similar two-stage relaxation behaviors at 1000, 1100, and 1200 °C.

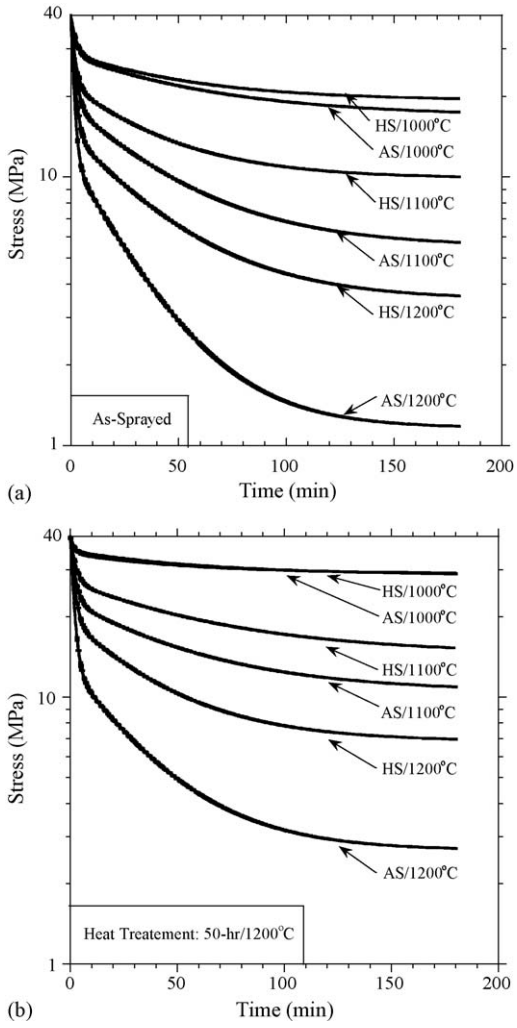

Fig. 5. (a) Comparison of stress–relaxation behavior of stand-alone as-sprayed coatings made from AS and HS powders as a function of test temperature. The initial stress in each coating was 40 MPa; (b) comparison of stress–relaxation behavior of stand-alone heat-treated coatings made from AS and HS powders as a function of test temperature. All heat treatments were conducted for 50 h at 1200 °C prior to testing. The initial stress in each coating was 40 MPa.

The amount of stress–relaxed in the as-sprayed condition was always greater than the amount of stress–relaxed after heat treatment at temperatures as low as 1000 °C for coatings made from both types of powders. For example, comparison of coatings prepared from HS powders tested at 1100 °C in the as-sprayed

Table 4
Curve fit parameter results for as-sprayed coatings made from AS and HS powders as a function of test temperature

Starting powder	Test temperature (°C)	Initial stress (MPa)	$w_1\sigma_0$ (MPa)	τ_1 (s)	$w_2\sigma_0$ (MPa)	τ_2 (s)	$w_3\sigma_0$ (MPa)	τ_3 (s)
AS	1000	40	11.8 ± 0.3	147 ± 12	11.3 ± 0.6	3693 ± 592	16.8 ± 0.8	3×10^8
	1100	40	21.5 ± 0	123 ± 20	13 ± 0.4	2634 ± 462	5.5 ± 0.4	3×10^8
	1200	40	28.3 ± 0.6	87 ± 6	10.5 ± 0.5	1677 ± 163	1.2 ± 0.3	1×10^8
HS	1000	40	11.3 ± 0.4	138 ± 4	9.5 ± 0.7	3205 ± 275	19.3 ± 0.4	1×10^9
	1100	40	18.2 ± 1	115 ± 23	11.9 ± 1.9	2425 ± 656	9.9 ± 1.2	2×10^8
	1200	40	25.5 ± 0.5	110 ± 9	11 ± 0.9	2365 ± 356	3.5 ± 0.5	7×10^7

Table 5
Curve fit parameter results for heat-treated coatings made from AS and HS powders as a function of test temperature

Starting powder	Test temperature (°C)	Initial stress (MPa)	$w_1\sigma_0$ (MPa)	τ_1 (s)	$w_2\sigma_0$ (MPa)	τ_2 (s)	$w_3\sigma_0$ (MPa)	τ_3 (s)
AS	1000	40	4.7 ± 0.8	87 ± 24	6.3 ± 0.3	3492 ± 443	29 ± 1	1×10^6
	1100	40	17.2 ± 0.3	133 ± 12	12.3 ± 0.3	3224 ± 363	10.5 ± 0.5	9×10^8
	1200	40	27.2 ± 0.8	108 ± 24	10.2 ± 1	2006 ± 371	2.7 ± 0.6	2×10^8
HS	1000	40	5.5 ± 0	120 ± 42	5.5 ± 0	3248 ± 25	29 ± 0	1×10^9
	1100	40	13 ± 2	143 ± 28	12.5 ± 1.3	3915 ± 958	14.5 ± 3.1	7×10^8
	1200	40	20.7 ± 0.8	118 ± 10	12.5 ± 1	2360 ± 104	6.8 ± 1	4×10^8

Coatings were heat-treated for 50 h at 1200 °C prior to testing.

condition (see Table 4) and after a 50 h heat treatment at 1200 °C (see Table 5) relaxed a total of 30.1 and 25.5 MPa, respectively, after 180 min. Note that the summation of $w_1\sigma_1$ and $w_2\sigma_2$ can be used to estimate the relaxation in 180 min. Similar trends were observed in coatings prepared from AS powders. Less stress–relaxation after heat treatment, even heat treatments as low as 1000 °C, have been attributed either loss of porosity or changes in the pore aspect ratios [25].

From Fig. 5a and b, it is apparent that as test temperature increases the extent of relaxation in the coatings prepared from AS powders increases as compared to coatings prepared from HS powders. Investigations by Dickinson et al. [16] on the effect of porosity on stress–relaxation of coatings showed a direct relationship between the amount of porosity and the amount of stress–relaxed. This was explained by the observation that a more porous microstructure would have less YSZ carrying the applied load. In this investigation, however, coatings made from higher porosity HS powders were found to relax less than coatings made from AS powders. As much of the additional porosity in coatings made from the HS powders was globular in shape, as a first approximation, it does not appear to affect the relaxation behavior significantly.

It is well established that a glassy phase can significantly affect the high-temperature properties of ceramics. For example, silicon nitride, with a thin layer of glass between the grains, shows a significant drop in strength as the test temperature approaches the glass transition temperature of the glass [26]. In the current research, the additional silica impurity in coatings made from AS powders (see Table 3) is believed to contribute significantly to the increased relaxation observed in coatings made from AS powders. This silica can combine with glass modifiers like CaO, which was also observed in the powders, to form a glass. In prior research [27], it was observed that presence of a glassy phase increased grain boundary sliding, a mechanism by which the stress is relaxed in the coating. From the current data set, it appears that even a slight increase in silica impurity content can strongly influence the stress–relaxation behavior of plasma-sprayed YSZ. In the current work, coatings made from AS powders had approximately 0.2 wt.% silica, twice that of the coatings made from HS powders. Thus, while the difference in silica content was small, the effect appears to have been large.

4. Conclusion

Coatings sprayed from two different powder types with similar composition, nominally 7 wt.% Y_2O_3–ZrO_2, were investigated. One of the coating types was prepared from an agglomerated and sintered (AS) powder, the other coating was prepared from a hollow-sphere (HS) powder produced by plasma densification. Microstructural characterization of as-sprayed specimens showed that coatings prepared from HS powders contained an extensive amount of globular porosity that was generated from the hollow morphology of the starting powders. Globular porosity was observed to be present after 50 h heat treatments at 1200 °C. Coatings prepared from AS powders contained significantly less globular porosity.

Thermal conductivity experiments showed that there was no statistical difference between the thermal conductivity of coatings prepared from either powder type in the as-sprayed condition and after a 50 h heat treatment at either 1000 and 1200 °C, despite the fact that coatings prepared from HS powders were more porous. It was proposed that the abundance of globular pores in coatings prepared from HS powders do not play a large role in reducing the overall thermal conductivity of the coating as compared to high-aspect ratio interlamellar pores. A 50 h heat treatment at 1400 °C resulted in a sharp increase in the thermal conductivity of coatings prepared from AS powders as compared to HS powders. This thermal conductivity increase in coatings made with AS powders was explained by enhanced sintering due to the presence of the silica impurity.

Compression stress–relaxation experiments on stand-alone coatings were conducted on coatings sprayed from both powder types. In general, all coatings showed two regime stress–relaxation behavior: an initial fast regime in the initial 10 min followed by a slower stress–relaxation behavior the rest of the test. Stress–relaxation of the original 40 MPa stress was observed to decrease when coatings made from both types of powders were heat-treated (1000, 1100, or 1200 °C for 50 h) prior to testing. Coatings prepared from AS powders relaxed more than coatings prepared from HS powders tested at identical conditions. This difference in behavior was attributed to the increased silica content in coatings made with AS powders. The presence of more glassy phase in the coatings made with AS powders is believed to increase grain boundary sliding, an active stress–relaxation mechanism.

Acknowledgements

Research sponsored by the Assistant Secretary for Energy Efficiency and Renewable Energy, Office of FreedomCAR and Vehicle Technologies, as part of the High Temperature Materials Laboratory, User Program, Oak Ridge National Laboratory, managed by UT-Batelle, LLC, for the U.S. Department of Energy under contract number DE-AC05-00OR22725.

References

[1] R.B. Heimann, Plasma-Spray Coating, Principles and Applications, Weinheim, New York, 1996.
[2] R.A. Miller, Surf. Coat. Tech. 30 (1987) 1–11.
[3] W. Beele, G. Marijnissen, A. Van Lieshout, Surf. Coat. Tech. 120 (1999) 61–67.
[4] R. McPherson, Surf. Coat. Tech. 39/40 (1989) 173–181.
[5] R. Trice, D. Prine, K. Faber, J. Am. Ceram. Soc. 83 (12) (2000) 3057–3064.
[6] J. Ilavsky, G.G. Long, A. Allen, C. Berndt, Mat. Sci. Eng. A 272 (1999) 215–221.
[7] J.S. Reed, Principles of Ceramic Processing, 2nd ed., Wiley Interscience, 1995, pp. 382–390.
[8] G. Pravdic, M.S.J. Gani, J. Mat. Sci. 31 (1996) 3487–3495.
[9] J. Ilavsky, J.K. Stalick, Surf. Coat. Tech. 127 (2000) 120–129.
[10] J.S. Wallace, J. Ilavsky, J. Thermal Spray Tech. 7 (4) (1998) 521–526.
[11] A.J. Allen, J. Ilavsky, G.G. Long, J.S. Wallace, C.C. Berndt, H. Herman, Acta Mater. 49 (2001) 1661–1675.
[12] R.W. Trice, Y.J. Su, K.T. Faber, H. Wang, W. Porter, Mat. Sci. Eng. A 272 (1999) 284–291.
[13] D. Zhu, R.A. Miller, Ceram. Eng. Sci. Proc. 23 (4) (2002) 457–468.
[14] S. Raghavan, H. Wang, W.D. Porter, R.B. Dinwiddie, M.J. Mayo, Acta Mater. 49 (2001) 169–179.
[15] A. Kulkarni, Z. Wang, T. Nakamura, S. Sampath, A. Goland, H. Herman, J. Allen, J. Ilavsky, G. Long, J. Frahm, R.W. Steinbrech, Acta Mater. 51 (2003) 2457–2475.
[16] G.R. Dickinson, C. Petorak, K.J. Bowman, R.W. Trice, J. Am. Ceram. Soc. 88 (8) (2005) 2202–2208.
[17] Standard Test Method for Water Adsorption, Bulk Density, Apparent Porosity and Apparent Specific Gravity of Fired Whiteware Products. ASTM C 373–88, 1999.
[18] J.B. Wachtman, Mechanical Properties of Ceramics, Wiley, New York, 1996, 392 pp.
[19] H. Wang, R.B. Dinwiddie, P.A. Gaal, Multiple station thermal diffusivity instrument, in: K.E. Wilkes, R.B. Dinwiddie, R.S. Graves (Eds.), Thermal Conductivity, vol. 23, Technomic Publishing, 1996, pp. 119–127.
[20] L.M. Clark III, R.W. Taylor, J. Appl. Phys. 46 (2) (1975) 714–719.
[21] H.E. Eaton, R.C. Novak, Surf. Coat. Tech. 32 (1987) 227–236.
[22] R. Vassen, N. Czech, W. Mallener, W. Stamm, D. Stover, Surf. Caot. Tech. 141 (2001) 135–140.
[23] K. Erk, C. Deschaseaux, R. Trice, J. Am. Ceram. Soc. 89 (5) (2006) 1673–1678.
[24] A.J. Allen, J. Ilavsky, G.G. Long, J.S. Wallace, C.C. Berndt, H. Herman, Acta Mater. 49 (2001) 1661–1675.
[25] C. Petorak, High temperature mechanical behavior of plasma-sprayed 7 wt.% yttria-stabilized zirconia stand-alone coatings, Purdue Masters Thesis, 2005.
[26] A.E. Pasto, W.C. Van Schalkwyk, F.M. Mahoney, Creep behavior of yttria- and alumina-doped silicon nitride, in: V.J. Tennery (Ed.), Proceedings of the Third International Symposium on Ceramic Components and Materials for Engines, American Ceramic Society, Westerville, OH, 1989, pp. 776–785.
[27] E.F. Rejda, D.F. Socie, T. Itoh, Surf. Coat. Tech. 113 (1999) 218–226.